

NUMERICAL SIMULATION OF INTERSECTING LINE WORKPIECE WELDED BY ARC ROBOT WELDING

Received – Primljeno: 2024-01-11

Accepted – Prihvaćeno: 2024-02-28

Original Scientific Paper – Izvorni znanstveni rad

Taking the pipe-pipe intersecting structure workpiece as the target, the Finite Element simulation (FEM) of the workpiece is carried out by using the finite element analysis software ABAQUS and the DFLUX subroutine. The temperature field and stress field during and after welding were studied to verify the welding process parameters and welding quality reliability of the welding workstation. The results show that the equivalent residual stress distribution of the weldment is consistent with the actual situation. Robot welding of complex welds is not only efficient, but also the welding quality is stable and reliable. This study provides a reference for the research of robot welding other complex workpieces.

Keywords: stell Q235; arc welding robot; stress; numerical simulation; ABAQUS

INTRODUCTION

Welding is an extremely important process in the manufacturing industry. With the continuous improvement of industrial robot industry technology, its function is more and more perfect, so the welding robot with good welding quality and high efficiency to perform welding tasks has gradually become the mainstream. [1] Among them, pipeline intersecting welding workpieces are widely used in petrochemical, power and other industries. The reliability and durability of its welding quality have become the main concerns. Therefore, this paper selects the pipe-to-pipe intersecting component weld of Q235 to complete the welding task by the welding robot MAG welding method. [2] The finite element method is used to analyze the temperature field and stress field during and after welding, and the reliability of robot welding is confirmed, which provides a reference for robot welding of complex space curve welds.

Arc-welding robot workstation

The arc welding robot workstation is shown in Figure 1, which includes ABB1660 robot body, workpiece fixture platform, control cabinet, welding power supply, wire feeding device, welding torch, protective gas cylinder and so on. In order to ensure the accurate tracking of the weld trajectory, based on the kinematic mapping of the joint space and the workspace, an advanced control algorithm is designed to suppress the model uncer-

tainty and compound disturbance in the robot dynamics to ensure the trajectory tracking accuracy of the robot.

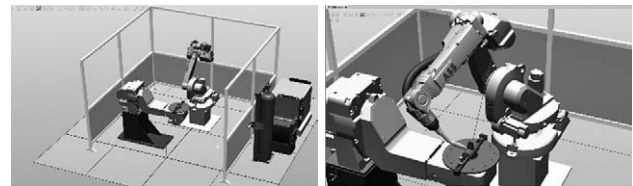


Figure 1 Welding robot workstation

Welding process parameters and FEM of workpiece

The chemical composition of ordinary carbon steel Q235 is shown in Table 1; The end of the robot clamps the gas metal arc welding torch (MAG), and the workpiece is constrained to be fixed at both ends of the main pipe. Before welding, the surface of the main pipe and branch pipe is polished to remove the oxide film and rust spot on the surface of the material, and the ABB arc welding robot is used for welding. The welding process parameters are shown in Table 2. [3]

The model is meshed according to the structure of the component. Without considering the deformation of

Table 1 Chemical composition of Q235 steel /wt.%

C	Si	Mn	P	S	Fe
≤ 0,22	≤ 0,35	≤ 0,3	≤ 0,045	≤ 0,045	residual

Table 2 Welding process parameters

Welding current/A	Arc voltage/V
220	26
Welding speed/mm · min ⁻¹	Wire feed rate/m · min ⁻¹
400	6

H.W. Wu, Y. Q. Cai (e-mail: caiyq@ncst.edu.cn), College of Mechanical Engineering, North China University of Science and Technology, Hebei, Tangshan, China.

the base metal, the C3D8R element type of linear reduction integral is selected. [4] The mesh division of the model is shown in Figure 2.

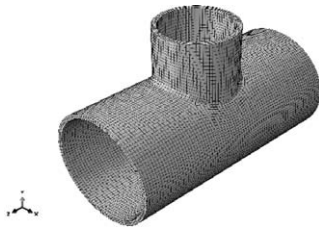


Figure 2 Mesh division of model

Based on the actual situation, the double ellipsoid heat source model is selected, as shown in the Figure3.

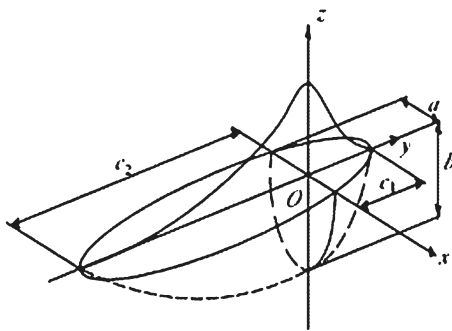


Figure 3 Double ellipsoid heat source model

The heat flux density function is expressed as:

$$\begin{cases} q_1(x, y, z) = \frac{6\sqrt{3}f_1Q}{abc_1\pi\sqrt{\pi}} \exp\left(-\frac{3x^2}{a^2} - \frac{3y^2}{b^2} - \frac{3z^2}{c_1^2}\right), z \ge 0 \\ q_2(x, y, z) = \frac{6\sqrt{3}f_2Q}{abc_2\pi\sqrt{\pi}} \exp\left(-\frac{3x^2}{a^2} - \frac{3y^2}{b^2} - \frac{3z^2}{c_2^2}\right), z \le 0 \end{cases}$$

In the formula, q_1, q_2 is the heat flux density at a certain position in the model, $Q = \eta UI$, η , is the welding thermal efficiency, U is the arc voltage, I is the welding current, a, b, c_1, c_2 is the heat source shape parameter, f_1, f_2 is the front and rear semi-ellipsoid energy distribution coefficient, and satisfies $f_1 + f_2 = 2$.

Numerical simulation results analysis

The Dflux subroutine is compiled by Fortran language. Under the relevant parameters such as welding voltage, current, thermal efficiency, welding speed, welding starting point coordinates and double ellipsoid heat source, the Dflux subroutine is associated with ABAQUS to realize the heat source loading of the welding process, and the temperature field and stress field are numerically simulated. [5]

The heat source trajectory of the weld during the welding process and the distribution of the temperature field at different times are shown in Figure 4. It shows the temperature field contours after 5 s, 10 s, 20,7s and 3 000 s cooling. It can be seen from the figure that under

the action of heat source, the heat diffuses along the weld, and the temperature of the component gradually increases. At this time, sufficient temperature accumulation has not yet been formed, and the maximum temperature near the heat source center is 2 700 °C. When the welding process is stable, the molten pool gradually moves forward with time, the temperature of each point near the molten pool is basically constant, and the shape of the molten pool remains basically unchanged, showing the characteristics of quasi-steady temperature field. After cooling, the temperature of the weldment has almost reached room temperature.

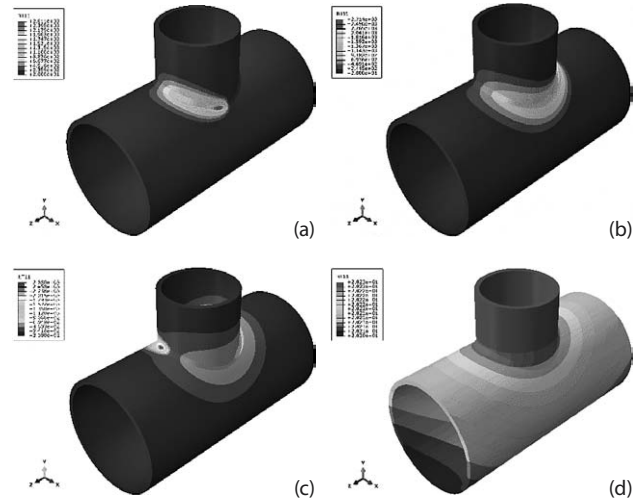


Figure 4 Results of weld temperature field model
(a) Welding time is 3 s (b) Welding time is 6 s
(c) Welding time is 9 s (d) Welding time is 3 000 s

The equivalent stress is studied and analyzed, and the equivalent stress field at 5 s, 15 s and cooling 3 000 s is selected as the research basis, see Figure 5. The equivalent stress is studied and analyzed4, and the equivalent stress field at 5 s, 15 s and cooling 3 000 s is selected as the research basis, see Figure 5. As the heat source continues to load, the temperature rises, the thermal expansion of the structure is constrained by the surrounding boundary conditions, and the equivalent stress of the component is close to the yield limit of the material. According to the change of the equivalent stress cloud map, the maximum Mises stress on the surface of the corresponding weldment at three times is : 213 MPa, 224 MPa, 284 MPa, and it can be obviously found that the equivalent stress value near the constraint area at both ends and near the weld area is larger.

The equivalent stress field after constraint removal is shown in Figure 6. The equivalent residual stress is evenly distributed and the maximum value is as high as 256 MPa.

The stress value in the vicinity of the weld is about 200 MPa; the equivalent residual stress gradually decreases from 256 MPa to about 100 MPa with the increase of the distance from the weld. The outermost equivalent residual stress is below 1 MPa.

The equivalent residual stress distribution on the two circumferential paths path1 and path2 on the upper

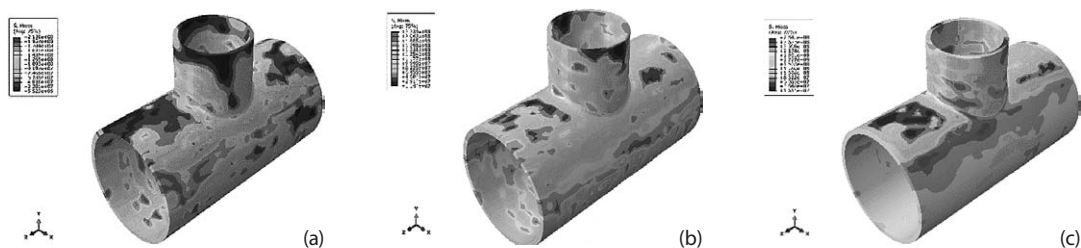


Figure 5 Results of weld stress field mode

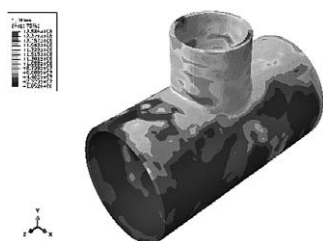
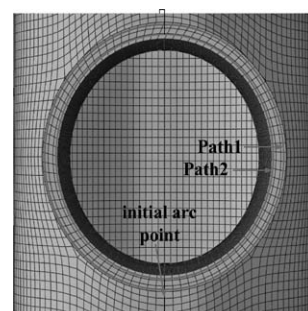
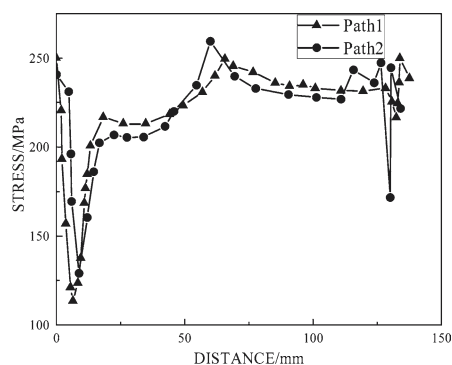


Figure 6 Equivalent stress field



(a)



(b)

Figure 7 Equivalent residual stress of circumferential path on weld surface

surface of the weld is shown in Figure 7. The equivalent residual stress distribution on the two paths ranges from 120 MPa to 260 MPa, and the equivalent residual stress at the starting point of welding is large, reaching about 240 MPa. Subsequently, the stress decreased rapidly and a trough appeared, and the equivalent residual stress decreased to 130 MPa. Then the stress increased sharply to 260 MPa, and then remained at this level. Finally, near the tail of the weld, that is, quickly back to the starting point, the equivalent residual stress fluctuates again. In Figure 5, there are two places where the equivalent residual stress fluctuates near the arc striking and closing positions, which is related to the constraints on the position of the weld.

CONCLUSION

Based on ABAQUS and DFLUX subroutines, the numerical simulation of the whole welding process was carried out by using the robot MAG welding Q235 material. In the welding process, with the effect of heat source, the distribution of welding temperature field and welding stress field at the joint of intersecting line is studied. After the welding is completed, after cooling and removing the constraints at both ends to release the stress, the residual stress is mainly distributed in the weld and its vicinity, and the maximum value reaches 258 MPa. Through the observation and analysis of the heat source shape, temperature field and stress field in the numerical simulation of welding, it is shown that the welding process parameters in the robot welding process are reasonable, and the welding task can be completed efficiently and high-quality, which makes an effective verification for the application of large quantities of welding robots in the market.

REFERENCE

- [1] Guo Y. B., Wang B., Wang D. G., et al. Research Progress and Development Trend of Welding Robot [J]. *Modern Manufacturing Engineering*, (2021) 05,53-63.
- [2] Lv M. M., Ji X. Q., The Influence of Different Process Parameters of MAG Welding on Weld Penetration of Welding Robot is Discussed [J]. *China Plant Engineering*, (2023) 21,124-126.
- [3] Ming C., Ma C. W., Numerical simulation and thermal cycle analysis of MAG welding temperature field based on ABAQUS [J]. *Electronic Science and Technology*, (2022) 35,74-78.
- [4] Zhang L., Wang Q., Chen P., et al. Finite Element Analysis of Restraint Intensities and Welding Residual Stresses in the Ti80 T-Joints [J]. *METALS*, (2023) 13,125.
- [5] De Arruda M. V., Correa E. O., Macanhan V. B. D. Optimization of FEM models for welding residual stress analysis using the modal method [J]. *Welding In the world*, (2023), 67: 2361-2372.

Note: The responsible translator for English language is J.W. Wang - NCST.